Matter and Radiation at Extremes | LETTER | scitation.org/journal/mre

# Generation of synchronized x-rays and mid-infrared pulses by Doppler-shifting of relativistically intense radiation from near-critical-density plasmas

Cite as: Matter Radiat. Extremes 8, 024001 (2023); doi: 10.1063/5.0116660
Submitted: 29 July 2022 • Accepted: 25 December 2022 •
Published Online: 2 February 2023



Nikita A. Mikheytsev[1,a] and Artem V. Korzhimanov[1,2,b]

## AFFILIATIONS

[1] Lobachevsky State University of Nizhny Novgorod, 603022 Nizhny Novgorod, Russia
[2] Federal Research Center Institute of Applied Physics of the Russian Academy of Sciences, 603950 Nizhny Novgorod, Russia

**Note:** This paper is a part of the Special Topic Collection on Plasma Optics.
[a] **Electronic mail:** mikheytsev@rf.unn.ru
[b] **Author to whom correspondence should be addressed:** artem.korzhimanov@ipfran.ru

## ABSTRACT

It is shown that when relativistically intense ultrashort laser pulses are reflected from the boundary of a plasma with a near-critical density, the Doppler frequency shift leads to generation of intense radiation in both the high-frequency (up to the x-ray) and low-frequency (mid-infrared) ranges. The efficiency of energy conversion into the wavelength range above 3 $\mu$m can reach several percent, which makes it possible to obtain relativistically intense pulses in the mid-infrared range. These pulses are synchronized with high harmonics in the ultraviolet and x-ray ranges, which opens up opportunities for high-precision pump–probe measurements, in particular, laser-induced electron diffraction and transient absorption spectroscopy.



## I. INTRODUCTION

The development of methods for generating and amplifying femtosecond laser pulses has led to the possibility of obtaining pulses with peak power up to several petawatts[1–4] and intensity above $10^{23}$ W/cm$^2$.[5,6] The interaction of such radiation with matter leads to efficient generation of charged particle beams[7,8] and radiation in various ranges.[9,10] In particular, much attention has been paid to the problem of generating high harmonics in the range of up to several keV from the surfaces of solid-density targets,[11,12] with efficiencies reaching tens of percent. In a number of papers, possible mechanisms for generating low-frequency radiation in the terahertz[13–22] and mid-infrared (mid-IR)[23–30] ranges have also been discussed, but, in general, these are still poorly understood.

Like the terahertz range, the mid-IR range, the lower limit of which we will consider to be 3 $\mu$m, is also poorly understood, owing to the fact that the radiation frequency here is too low for efficient laser generation, but too high for electronic generation methods. However, in recent years, there has been a sharp increase in the efficiency of sources in this range based on parametric amplification of light. Peak pulse powers at the sub-terawatt level have now been reached in the range of 3–4 $\mu$m[31] and at the gigawatt level in the range of 5–9 $\mu$m,[32] which has made it possible to achieve relativistic intensities and, in particular, to demonstrate the generation of relativistic high harmonics.[33–35]

In spite of their scarcity, mid-IR sources are in great demand for a large number of spectrographic applications.[36] In particular, they are of interest for use in laser-induced electron diffraction, in which the electronic configuration of a molecule is determined by the diffraction signal from an electron of the same molecule, ionized by a powerful mid-IR pulse and scattered by the molecule during reverse motion.[37] In pump–probe experiments with controlled delay, this makes it possible to study the dynamics of the electronic configuration with femtosecond time resolution. The pump

can be provided by (among other things) ultraviolet or x-ray radiation, which produce either ionization or excitation of the molecule. Sub-femtosecond synchronization of low- and high-frequency radiation is also needed in the case of transient absorption spectroscopy, in which an object is excited by a mid-IR pulse and short-duration ultraviolet radiation is used as a probe.[38,39] Thus, synchronized sources of high- and low-frequency radiation of high intensity are in demand.

In this work, we take account of the fact that, along with the generation of high harmonics, when intense laser radiation is reflected from a plasma surface, generation of low-frequency radiation is also observed. The underlying mechanism is, in fact, the same, namely, the Doppler frequency shift. However, unlike high harmonics, which are observed when the boundary moves toward the laser radiation, the low-frequency pulses are observed when it moves toward the plasma. Although the generation of low-frequency radiation has been reported previously,[40,41] it has not attracted much attention, apparently because of the low efficiency of generation in most cases, which is a consequence of the low velocity with which the boundary moves toward the plasma, in contrast to the velocity of its outward motion, which easily reaches relativistic values.

To increase the efficiency of generation in the wavelength range above 3 $\mu$m, we propose the use of near-critical-density targets, which have already been successfully used in various experiments with high-intensity laser pulses.[42–47] Reducing the target density to a near-critical value leads to an increase in the velocity of the boundary motion without a decrease in the reflection efficiency in terms of the number of reflected photons. A simple estimate shows that if the maximum speed is reached for a time of about $\alpha = 1/10$ of the laser radiation period in the reference frame associated with the plasma boundary, and the ratio of the incident laser frequency to the Doppler-shifted one is about $\delta = 5$, then for a laser pulse with a wavelength of 0.8 $\mu$m, the energy efficiency of conversion to the 4 $\mu$m wavelength range will be about $\alpha/\delta = 0.02$, which for an incident pulse with an energy of about 10 J will give a mid-IR pulse with an energy of 0.2 J. Assuming that the reflected pulse will have a duration of the order of that of the driving pulse, namely, 50 fs, we get a power estimate of 4 TW. For a transverse pulse size of about 4 $\mu$m, the intensity will be about $10^{18}$ W/cm$^2$, and the dimensionless relativistic parameter is $a_{\mathrm{mIR}} = (e\lambda/m_e c^2)\sqrt{2I/\pi c} = \lambda\ (\mu\mathrm{m})\sqrt{I\ (\mathrm{W/cm^2})/1.38\times 10^{18}} \approx 3.4$ (where $c$, $e$, and $m_e$ are the speed of light, the elementary charge, and the mass of the electron, respectively, and $\lambda$ and $I$ are the wavelength and intensity, respectively, of the radiation), which is higher than the record values achieved to date. This pulse will be automatically synchronized to sub-femtosecond precision with high harmonics, allowing them to be used together in high-precision pump–probe experiments. At the same time, the high radiation power makes it possible to perform measurements in a large volume of matter, increasing the diffraction signal.

## II. RELATIVISTIC ELECTRON SPRING MODEL

Let us consider the process of radiation generation at the boundary of a plasma irradiated by a short relativistically intense linearly polarized laser pulse. For the sake of clarity, we restrict ourselves to the one-dimensional (1D) case along the $x$ axis with normal incidence of the laser pulse from the region $x < 0$. Since we are also interested in a near-critical-density plasma, in which internal plasma fields can play a significant role, the most suitable approach for theoretical analysis is to adopt the relativistic electron spring model proposed in Ref. 48 and developed in Ref. 49.

The relativistic electron spring model is based on three relatively simple approximations, which can be justified by comparison with the results of fully electrodynamic kinetic numerical simulations. First, the ultrarelativistic limit is considered, in which electrons can have a speed equal to either zero or the speed of light. Second, it is assumed that the plasma at any moment of time consists of a stationary ion background occupying the region $x > 0$, an infinitely thin electron layer at the point $x = x_s(t)$, containing all the electrons squeezed out by the ponderomotive pressure from the region $0 < x < x_s(t)$, and unperturbed electrons in the rest of the space $x > x_s(t)$. Third, it is assumed that the incident field and the field emitted by the electron layer exactly compensate for each other in the region $x > x_s(t)$, which allows us to write the equation of motion of the electron layer as[49]

$$\frac{dx_s}{dt} = \frac{f^2(x_s - t) - (n_0 x_s/2)^2}{f^2(x_s - t) + (n_0 x_s/2)^2}, \tag{1}$$

where relativistic units are used: $f(\xi) = e|\mathbf{E}_\perp(\xi)|/m_e\omega c$ is the value of the transverse electric field of the incident wave, $n_0 = 4\pi e^2 N_e/m\omega^2$ is the unperturbed concentration of electrons in the plasma (the plasma is assumed to be initially homogeneous for simplicity), and distances are measured in $c/\omega$ and time intervals in $\omega^{-1}$, where $\omega$ is some frequency, which we choose equal to the carrier frequency of the incident radiation.

With a known laser pulse shape $f(x - t)$, Eq. (1) can be integrated numerically. Knowing the position of the layer at each moment of time and determining the currents in it based on the assumptions of the model, we can calculate the reflected radiation:[49]

$$f^r(x_s(t) + t) = -\frac{1 - \beta_x}{1 + \beta_x} f(x_s(t) - t), \tag{2}$$

where $f^r(x + t)$ is the electric field of the reflected pulse and $\beta_x = dx_s/dt$ is the longitudinal velocity of the electron layer.

Figure 1 shows an example of a solution of Eq. (1), together with the corresponding forms of the incident and reflected pulses, calculated using Eq. (2). Under the influence of ponderomotive pressure, the electron boundary oscillates, and during the return motion its speed at some moments of time almost reaches the speed of light. At these times, the most efficient generation of high harmonics occurs, which sharp peaks with a sub-femtosecond duration in the reflected field. Those peaks are easily recognized in Fig. 1(c): three between $t = 3$ fs and $t = 9$ fs generated during the average motion of the pulse toward the plasma and three after $t = 10$ fs during the average motion of the pulse outward from the plasma when the laser pulse has become extinct. It should be noted that these peaks are infinite, which is due to the prescribed infinitesimally small thickness of the reflected electron layer and its consequent infinitely large density. Along with this, however, there is an average motion of the boundary deep into the plasma with a velocity of the order of 0.5$c$–0.6$c$. This movement should also lead to an enrichment of the spectrum of the reflected signal in the low-frequency region. It can also be expected that the efficiency of generation of a low-frequency signal,

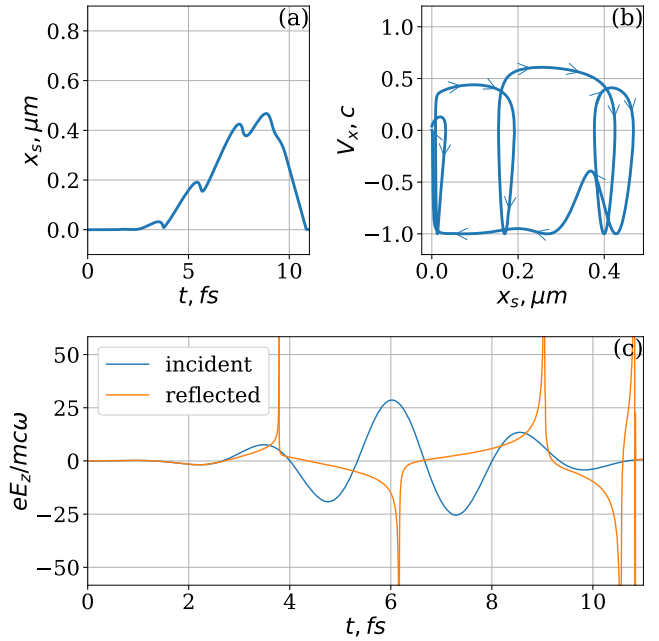


**FIG. 1.** Solution of the equations of the relativistic electron spring model for a Gaussian pulse of duration 3 fs and amplitude $a_0 = 30$ and a homogeneous plasma of density $n_0 = 10$. (a) Trajectory of the electron boundary $x_s(t)$. (b) Trajectory of the electron boundary in phase space $(x, v_x = dx/dt)$. (c) Temporal profiles of the incident (blue) and reflected (orange) pulses.

as well as its wavelength, will increase with an increase in this speed. Such an increase can be achieved either by increasing the laser pulse amplitude or by decreasing the plasma density. Thus, it can be expected that it will be more optimal to use plasma of near-critical density, which, on the one hand, is still opaque and is able to effectively reflect radiation, and, on the other hand, makes it possible to achieve the maximum boundary velocity.

## III. PARTICLE-IN-CELL SIMULATIONS

To test the predictions of the theoretical model and study the interaction process in the range of parameters in which the model is not applicable, we performed numerical simulations based on the particle-in-cell (PIC) method. For these purposes, the PICADOR package was used, which implements the fully electrodynamic relativistic PIC method.[50] We first present the results of 1D calculations and then discuss the features of the multidimensional problem.

The simulations were carried out in a box 40 $\mu$m in size with a grid step $\Delta x = 2.5$ nm. The time step was $\Delta t = \Delta x/2c \approx 4.2$ as. The plasma at the initial moment of time was set as a layer with a uniform concentration of particles 10 $\mu$m long, with 50 macroparticles in the cell. Its left boundary was initially at 30 $\mu$m from the left boundary of the box. Ions were considered immobile for clarity and because of the short interaction time. The electron temperature at the initial moment of time was set equal to 100 eV, which is much less than the energy of electron motion in the field of the incident wave. The total simulation time was 150 fs, which was sufficient to observe the entire interaction process, as well as the subsequent plasma emission. The parameters of laser radiation corresponded to a Gaussian pulse at a wavelength of 800 nm with an energy of 10 J and a duration of 20 fs at full width at half maximum (FWHM) of the intensity, focused into a spot with a diameter of 5 $\mu$m. For these parameters, the amplitude of the incident pulse is $a_0 = 27.85$.

Figure 2 shows a typical result of a 1D calculation for the plasma density $n_0 = 30$. It can be seen that under the action of incident radiation, the plasma boundary undergoes oscillations of significant amplitude with a gradually averaged movement deep into the plasma. Spectral filtering of the reflected pulse shows the presence of high-energy harmonics in it, as well as a low-frequency signal. The low-frequency signal filtered in the wavelength range above 3 $\mu$m reaches an amplitude $E \approx 0.5 m_e c\omega/e \approx 2$ TV/m in the given case, which corresponds to a normalized relativistic value $a_{\mathrm{mIR}} = eE/(m_e c\omega_{3\mu\mathrm{m}}) \approx 1.9$, where $\omega_{3\mu\mathrm{m}}$ is the frequency corresponding to a wavelength of 3 $\mu$m. Note that the wavelength in this range significantly exceeds the duration of the time intervals during which the boundary motion velocity is positive, and so this signal is determined mainly by the envelope of the incident laser pulse, and not by the details of the boundary motion.

To confirm the Doppler mechanism of low-frequency radiation generation, we performed a direct comparison of the spectra of reflected signals obtained within the framework of the relativistic electron spring model and from calculations, shown in Fig. 3. The Fourier spectra in the PIC simulations were taken for spatial distributions of the magnetic field. Note the good qualitative agreement between these spectra. Some discrepancy is explained by the fact that, strictly speaking, the model of a relativistic electron

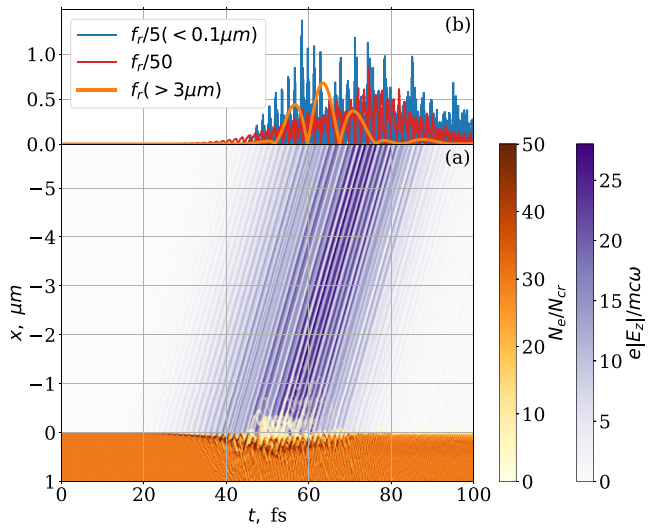


**FIG. 2.** Result of a 1D PIC simulation for a Gaussian laser pulse of duration 20 fs and amplitude $a_0 = 27.85$ and a homogeneous plasma of density $n_0 = 30$. (a) Spatiotemporal dynamics of the electron concentration (orange) and reflected radiation (violet). The concentration is normalized to the critical concentration for the carrier frequency of the incident laser pulse $N_{cr} = m\omega^2/4\pi e^2$. (b) Time profile of the reflected pulse without filtering (red), after filtering in the <0.1 $\mu$m wavelength range (blue), and after filtering in the <3 $\mu$m wavelength range (orange). The field is normalized to $m_e c\omega/e$.

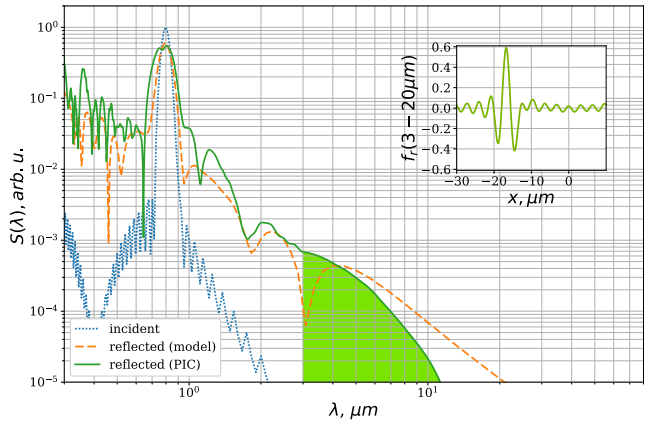


**FIG. 3.** Comparison of Fourier spectra for the incident pulse (blue dotted line), the reflected pulse obtained from the relativistic electron spring model (orange dashed line), and the reflected pulse obtained from the 1D PIC simulation (green full line). The inset shows the time profile of the pulse obtained after filtering the reflected signal in the 1D PIC simulation in the range 3–20 $\mu$m. The simulation parameters are the same as in Fig. 2.

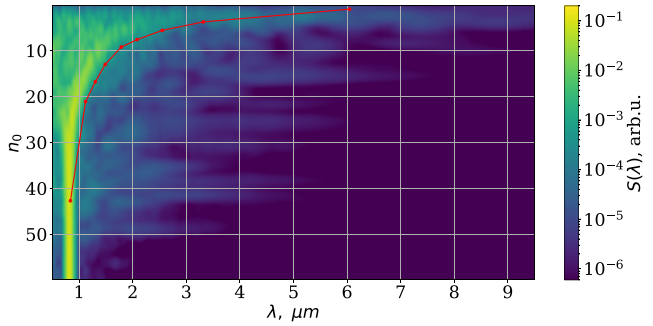


**FIG. 4.** Dependence of the Fourier spectrum of the reflected signal obtained in 1D PIC simulation of the plasma density. The data shown are for a laser pulse amplitude $a_0 = 27.85$ and a duration of 20 fs. The red line corresponds to a Doppler shift induced by a mirror moving at the velocity of the laser front penetrating into the plasma as estimated from the simulations.

spring is not applicable in the parameter range under study, since at $n_0/a_0 \sim 1$, signs of relativistic self-induced transparency begin to appear and some of the electrons begin to fly out of the plasma toward the laser radiation, as can be seen in Fig. 2 at a time $t \approx 50$ fs. This leads to a violation of the assumption that there are no electrons in the region $x < x_s(t)$. Nevertheless, the proximity of the spectra obtained within the framework of the model and from the simulation allows us to conclude that the model correctly captures the main mechanism of low-frequency radiation generation and that since the model is purely electrodynamic, this mechanism is the Doppler effect.

Figure 3 also shows the shape of the filtered mid-IR pulse. This pulse contains several field oscillations, although there are fewer of these than in the incident pulse. Thus, after filtering, it is possible to obtain an extremely short pulse with relativistic amplitude.

One might think that it is the threshold of the induced transparency that determines the optimal plasma density at which the maximum efficiency of low-frequency radiation generation is observed, but our analysis has shown that this is not the case.

Figure 4 shows the dependence of the reflected signal spectrum on the plasma density. Indeed, for $n_0 < a_0$, a strong modification of this spectrum is observed. An increase in the spectral width, an increase in the maximum generated wavelength, and a shift of the spectral maximum to the long-wavelength region are observed. However, it should be noted that the position of the spectral maximum does not exceed 3 $\mu$m, even for $n_0 \sim 1$, and thus does not enter the mid-IR region. Despite these changes, the total radiation power in the long-wavelength region does not decrease with a decrease in density in the range $1 < n_0 < a_0$. This can be seen from the radiation energy integrated over the range $\lambda > 3$ $\mu$m, whose dependence on the plasma density is shown in Fig. 5.

This behavior can be explained by the fact that, as has been noted previously,[51–54] induced transparency at a sharp plasma boundary manifests itself in the appearance of electron beams breaking off toward the incident laser radiation. This is accompanied by a deeper penetration of the radiation into the plasma. However, if the plasma density is not too low, this process inevitably stops, and later the laser radiation is completely reflected. Even after the disruption, the reflective electron layer is not completely destroyed and continues to reflect radiation. Therefore, generation of low-frequency radiation is also observed in this case, and its efficiency does not decrease.

It should be noted, however, that for a sufficiently low $n_0 < 1$, the radiation begins to penetrate into the plasma continuously, total reflection does not occur, and the efficiency of the Doppler generation mechanism here becomes low. Figure 5 also shows the dependence of the total reflected energy on the plasma

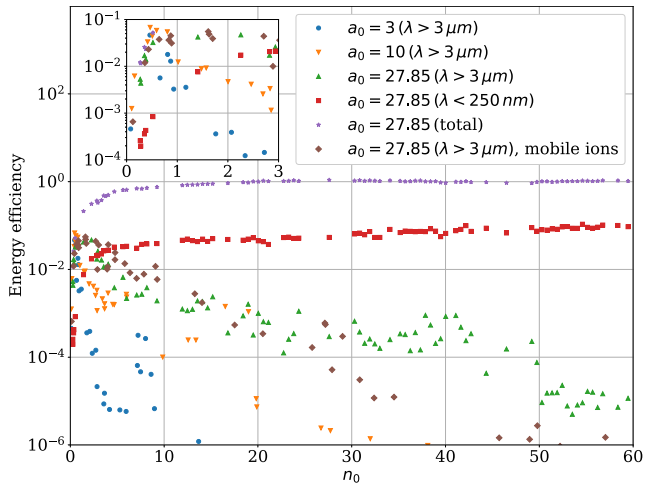


**FIG. 5.** Dependence of the energy efficiency of the conversion of the incident laser radiation into the reflected signal in different ranges for different amplitudes of the pulse. The results are shown for 1D PIC simulations with immobile ions. For comparison, the result for the case of mobile ions is also presented. The laser pulse duration is 20 fs, and its amplitude is given in the legend.

density. It can be seen that it almost equals unity down to $n_0 \sim 5$ and begins to decline for lower densities. A sharp decrease in reflection is observed, however, only for $n_0 < 0.5$. It turns out to be optimal to use a plasma with a density $n_0 \approx 0.5$–1, at which conversion of up to 5% of the incident energy into radiation energy with a wavelength greater than 3 $\mu$m is achieved. This result agrees well with the rough estimate we gave at the beginning.

Figure 5 also shows the efficiency of generation of long-wavelength radiation at lower laser pulse amplitudes. It can be seen that the efficiency decreases with a decrease in the amplitude. However, at the optimum plasma density, even at a relatively small amplitude $a_0 = 3$, the efficiency still reaches several percent. Simultaneously, the range of densities at which the efficiency exceeds a certain level becomes narrower with decreasing amplitude.

Up to now, it has been assumed that the ions are immobile. This has been done primarily for simplicity and clarity of presentation. At the same time, we do not expect ions to play a significant role in the mechanism under discussion, although they can slightly modify the results of the analysis. This is due to the fact that relatively short pulses and relatively low plasma densities are considered. Indeed, the ion response time is of the order of the reverse ion frequency $\omega_{pi}^{-1} = [M_i/(4\pi Z_i e^2 N_e)]^{1/2}$ (where $M_i$ and $Z_i$ are the ion mass and charge state, respectively), which in the case of protons and a density of $n_0 = 10$ is about 12 periods of the laser field. For heavier ions and lower plasma densities, this number will be even higher, while pulses with a duration of 30–50 fs, typical of experiments, contain just 10–20 cycles. To confirm the weakness of the influence of the ionic component on the ongoing processes, Fig. 5 shows for comparison the efficiency of long-wavelength radiation generation in the case of mobile ions with a charge-to-mass ratio $Z_i/M_i = 1$, corresponding to protons. It can be seen that the ions start to play a role only at densities higher than $n_0 > 30$.

From the point of view of applications requiring both low- and high-frequency pulses, a potential disadvantage may be that the increase in the efficiency of low-frequency generation with decreasing plasma density is accompanied by a decrease in the efficiency of high-harmonic generation. This is due to the fact that the generation of harmonics requires the movement of plasma electrons toward the radiation, while at sufficiently low densities, electrons can move inward toward the plasma almost continuously. To investigate this effect, Fig. 5 also shows the efficiency of generation of short wavelengths. As expected, it can be seen that as the density decreases, this efficiency gradually decreases, and at $n_0 < 2$ it becomes less than 1%, after which it drops sharply. However, there is a density range $n_0 = 2$–5 in which the efficiency of generating both low- and high-frequency radiation exceeds 1% and which can be used for the simultaneous efficient generation of pulses in the mid-IR and ultraviolet ranges.

We would also like to note that at low densities, mechanisms other than the Doppler effect can contribute to the generation of long wavelengths, namely, backward stimulated Raman scattering (BSRS) and nonlinear self-phase modulation, which have been discussed previously.[55,56] We are not going to investigate the relative roles of these mechanisms in detail here; however, we do not expect them to dominate in the mid-IR range for our parameters. First, as follows from reported simulations, even in near-critical-density targets, the peak of generation is above $\omega/3$.[57] Second, the efficiency of BSRS drops rapidly at laser pulse durations less than the plasma wavelength. In the case of $n_0 \sim 1$ and $a_0 \sim 30$, the relativistically corrected plasma wavelength can be estimated as $\lambda_p^{\mathrm{rel}} = (\pi\sqrt{1+a_0^2}\, m_e c^2/e^2 N_e)^{1/2} \approx (a_0/n_0)^{1/2}\lambda_L \approx 5.5\lambda_L$ (where $\lambda_L$ is the laser wavelength), whereas the laser pulse in our simulations contained only seven to eight optical cycles. For lower amplitudes and longer pulses, however, the contribution of BSRS can be more pronounced. Finally, we tried to compare the measured spectra with what would be expected from the Doppler effect. For this, we estimated the average velocity of the laser front penetrating into the plasma and calculated the Doppler shift expected from a mirror moving at this velocity. The result is shown in Fig. 4 and it reveals a good coincidence. This allows us to suppose that

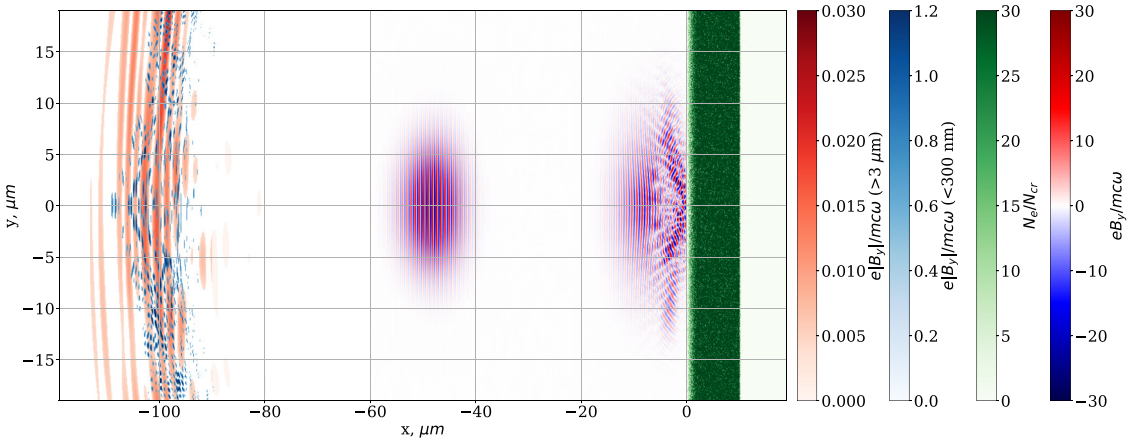


**FIG. 6.** Result of a 2D PIC simulation of the interaction of a Gaussian pulse of duration 20 fs, width 5 $\mu$m, and amplitude $a_0 = 27.85$ with a plasma of density $n_0 = 30$, which has a preplasma layer of thickness 2 $\mu$m with a linear density gradient. In the center is shown the laser pulse at the beginning of the calculation. On the right are shown the transverse fields and the electron density at time $t = 200$ fs after the start of the calculation. On the left are shown the low-frequency (in the wavelength range >3 $\mu$m, red) and high-frequency (in the wavelength range <300 nm, blue) parts of the reflected pulse at time $t = 550$ fs after the start of the calculation.

the Doppler mechanism plays the main role, even at relatively low densities.

## IV. 2D PIC SIMULATIONS

One-dimensional modeling makes it possible, on the one hand, to highlight the most important physical mechanisms responsible for the observed effects, and, on the other hand, to carry out a relatively fast multiparameter study. However, in reality, it is difficult to create conditions close to one-dimensional, in particular because of the need to use relatively sharp focusing to achieve the desired intensities, and also because of the possible development of transverse instabilities. To confirm that these features do not fundamentally affect the result obtained in the 1D analysis, we also carried out a two-dimensional (2D) calculation using the same fully electrodynamic kinetic PIC method implemented in the PICADOR package.

In this calculation, the box size was $140 \times 60$ $\mu$m$^2$, with a computational grid of $7000 \times 3000$ points. The time step was $\Delta t = \Delta x/2c \approx 33$ as. The plasma at the initial moment of time consisted of a homogeneous layer of density $n_0 = 30$ and thickness 10 $\mu$m and a preplasma layer in which the density increased linearly from $n_0 = 0$ to $n_0 = 30$ at a distance of 2 $\mu$m. The preplasma layer started at a distance of 120 $\mu$m from the left boundary of the box. The preplasma layer mimics the influence of a possible prepulse in the experiment. The ions were mobile, and their charge-to-mass ratio was equal to unity, corresponding to protons. There were ten macroparticles in the cell. The electron temperature at the initial moment of time was set equal to 100 eV. The total simulation time was 1.5 ps. The incident pulse had a wavelength of 800 nm and a Gaussian shape with a duration of 20 fs at FWHM, and it was focused on the surface of the plasma layer in a spot with a diameter of 5 $\mu$m at FWHM. The pulse energy was assumed to be 10 J, which corresponds to an amplitude at the focus of $a_0 = 27.85$ and an intensity of $1.7 \times 10^{21}$ W/cm$^2$.

The results of the calculation are shown in Fig. 6. Note that, as in the 1D case, efficient generation of both high-frequency bursts and low-frequency radiation containing several field oscillations is observed. Owing to diffraction, however, the amplitude of the low-frequency signal turns out to be lower than in the 1D case, and, in addition, a rather strong divergence of this signal is observed, caused by the relatively small focusing radius of the laser pulse and the consequent small size of the emitter compared with the generated wavelength. Nevertheless, the main effect is retained in the 2D case, which allows us to hope for the possibility of successful experimental demonstration as well.

## V. CONCLUSIONS

We have proposed a new scheme for the simultaneous generation of x-ray and mid-IR pulses internally synchronized with sub-femtosecond accuracy. This scheme is based on the well-known method of Doppler frequency conversion in the interaction of relativistically intense laser pulses with the surfaces of overdense plasma targets. Owing to the use of near-critical density targets, the efficiency of mid-IR pulse generation can be greatly increased and can reach several percent in energy. The generated mid-IR pulses have only a few optical cycles and can reach relativistic amplitudes exceeding the record values achieved to date by alternative methods.

Simultaneous generation of high-power synchronized x-ray and mid-IR pulses can be required for pump–probe experiments, for example, laser-induced electron diffraction with increased accuracy.

## ACKNOWLEDGMENTS

This research was supported by the Ministry of Science and Higher Education of the Russian Federation, state assignment for the Lobachevsky University of Nizhny Novgorod, Project No. 0729-2020-0035, and state assignment for the Institute of Applied Physics RAS, Project No. 0030-2021-0012. The simulations were performed on resources provided by the Joint Supercomputer Center of the Russian Academy of Sciences.

## AUTHOR DECLARATIONS

### Conflict of Interest

The authors have no conflicts to disclose.

### Author Contributions

**Nikita A. Mikheytsev**: Software (lead); Visualization (lead); Writing – review & editing (equal). **Artem V. Korzhimanov**: Conceptualization (lead); Funding acquisition (lead); Project administration (lead); Supervision (lead); Writing – original draft (lead); Writing – review & editing (equal).

## DATA AVAILABILITY

The data that support the findings of this study are available from the corresponding author upon reasonable request.

## REFERENCES

[1] C. Danson, D. Hillier, N. Hopps, and D. Neely, "Petawatt class lasers worldwide," High Power Laser Sci. Eng. **3**, e3 (2015).
[2] J. H. Sung, H. W. Lee, J. Y. Yoo, J. W. Yoon, C. W. Lee, J. M. Yang, Y. J. Son, Y. H. Jang, S. K. Lee, and C. H. Nam, "4.2 PW, 20 fs Ti:sapphire laser at 0.1 Hz," Opt. Lett. **42**, 2058 (2017).
[3] F. Lureau, G. Matras, O. Chalus, C. Derycke, T. Morbieu, C. Radier, O. Casagrande, S. Laux, S. Ricaud, G. Rey, A. Pellegrina, C. Richard, L. Boudjemaa, C. Simon-Boisson, A. Baleanu, R. Banici, A. Gradinariu, C. Caldararu, B. D. Boisdeffre, P. Ghenuche, A. Naziru, G. Kolliopoulos, L. Neagu, R. Dabu, I. Dancus, and D. Ursescu, "High-energy hybrid femtosecond laser system demonstrating $2 \times 10$ PW capability," High Power Laser Sci. Eng. **8**, e43 (2020).
[4] C. Radier, O. Chalus, M. Charbonneau, S. Thambirajah, G. Deschamps, S. David, J. Barbe, E. Etter, G. Matras, S. Ricaud, V. Leroux, C. Richard, F. Lureau, A. Baleanu, R. Banici, A. Gradinariu, C. Caldararu, C. Capiteanu, A. Naziru, B. Diaconescu, V. Iancu, R. Dabu, D. Ursescu, I. Dancus, C. A. Ur, K. A. Tanaka, and N. V. Zamfir, "10 PW peak power femtosecond laser pulses at ELI-NP," High Power Laser Sci. Eng. **10**, e21 (2022).
[5] J. W. Yoon, C. Jeon, J. Shin, S. K. Lee, H. W. Lee, I. W. Choi, H. T. Kim, J. H. Sung, and C. H. Nam, "Achieving the laser intensity of $5.5 \times 10^{22}$ W/cm$^2$ with a wavefront-corrected multi-PW laser," Opt. Express **27**, 20412 (2019).
[6] J. W. Yoon, Y. G. Kim, I. W. Choi, J. H. Sung, H. W. Lee, S. K. Lee, and C. H. Nam, "Realization of laser intensity over $10^{23}$ W/cm$^2$," Optica **8**, 630 (2021).

[7]E. Esarey, C. B. Schroeder, and W. P. Leemans, "Physics of laser-driven plasma-based electron accelerators," Rev. Mod. Phys. **81**, 1229–1285 (2009).
[8]A. Macchi, M. Borghesi, and M. Passoni, "Ion acceleration by superintense laser-plasma interaction," Rev. Mod. Phys. **85**, 751 (2013).
[9]S. Corde, K. Ta Phuoc, G. Lambert, R. Fitour, V. Malka, A. Rousse, A. Beck, and E. Lefebvre, "Femtosecond x rays from laser-plasma accelerators," Rev. Mod. Phys. **85**, 1–48 (2013).
[10]F. Albert and A. G. R. Thomas, "Applications of laser wakefield accelerator-based light sources," Plasma Phys. Controlled Fusion **58**, 103001 (2016).
[11]B. Dromey, S. Kar, C. Bellei, D. C. Carroll, R. J. Clarke, J. S. Green, S. Kneip, K. Markey, S. R. Nagel, P. T. Simpson, L. Willingale, P. McKenna, D. Neely, Z. Najmudin, K. Krushelnick, P. A. Norreys, and M. Zepf, "Bright multi-keV harmonic generation from relativistically oscillating plasma surfaces," Phys. Rev. Lett. **99**, 085001 (2007).
[12]U. Teubner and P. Gibbon, "High-order harmonics from laser-irradiated plasma surfaces," Rev. Mod. Phys. **81**, 445–479 (2009).
[13]J. Yoshii, C. H. Lai, T. Katsouleas, C. Joshi, and W. B. Mori, "Radiation from Cerenkov wakes in a magnetized plasma," Phys. Rev. Lett. **79**, 4194–4197 (1997).
[14]W. P. Leemans, C. G. Geddes, J. Faure, C. Tóth, J. van Tilborg, C. B. Schroeder, E. Esarey, G. Fubiani, D. Auerbach, B. Marcelis, M. A. Carnahan, R. A. Kaindl, J. Byrd, and M. C. Martin, "Observation of terahertz emission from a laser-plasma accelerated electron bunch crossing a plasma-vacuum boundary," Phys. Rev. Lett. **91**, 074802 (2003).
[15]A. Gopal, S. Herzer, A. Schmidt, P. Singh, A. Reinhard, W. Ziegler, D. Brömmel, A. Karmakar, P. Gibbon, U. Dillner, T. May, H. G. Meyer, and G. G. Paulus, "Observation of gigawatt-class THz pulses from a compact laser-driven particle accelerator," Phys. Rev. Lett. **111**, 074802 (2013).
[16]G. Q. Liao, Y. T. Li, C. Li, L. N. Su, Y. Zheng, M. Liu, W. M. Wang, Z. D. Hu, W. C. Yan, J. Dunn, J. Nilsen, J. Hunter, Y. Liu, X. Wang, L. M. Chen, J. L. Ma, X. Lu, Z. Jin, R. Kodama, Z. M. Sheng, and J. Zhang, "Bursts of terahertz radiation from large-scale plasmas irradiated by relativistic picosecond laser pulses," Phys. Rev. Lett. **114**, 255001 (2015).
[17]G.-Q. Liao, Y.-T. Li, Y.-H. Zhang, H. Liu, X.-L. Ge, S. Yang, W.-Q. Wei, X.-H. Yuan, Y.-Q. Deng, B.-J. Zhu, Z. Zhang, W.-M. Wang, Z.-M. Sheng, L.-M. Chen, X. Lu, J.-L. Ma, X. Wang, and J. Zhang, "Demonstration of coherent terahertz transition radiation from relativistic laser-solid interactions," Phys. Rev. Lett. **116**, 205003 (2016).
[18]K. B. Kwon, T. Kang, H. S. Song, Y.-K. Kim, B. Ersfeld, D. A. Jaroszynski, and M. S. Hur, "High-energy, short-duration bursts of coherent terahertz radiation from an embedded plasma dipole," Sci. Rep. **8**, 145 (2018).
[19]J. Déchard, A. Debayle, X. Davoine, L. Gremillet, and L. Bergé, "Terahertz pulse generation in underdense relativistic plasmas: From photoionization-induced radiation to coherent transition radiation," Phys. Rev. Lett. **120**, 144801 (2018).
[20]S. Herzer, A. Woldegeorgis, J. Polz, A. Reinhard, M. Almassarani, B. Beleites, F. Ronneberger, R. Grosse, G. G. Paulus, U. Hübner, T. May, and A. Gopal, "An investigation on THz yield from laser-produced solid density plasmas at relativistic laser intensities," New J. Phys. **20**, 063019 (2018).
[21]J. Déchard, X. Davoine, and L. Bergé, "THz generation from relativistic plasmas driven by near- to far-infrared laser pulses," Phys. Rev. Lett. **123**, 264801 (2019).
[22]Y. Zeng, C. Zhou, L. Song, X. Lu, Z. Li, Y. Ding, Y. Bai, Y. Xu, Y. Leng, Y. Tian, J. Liu, R. Li, and Z. Xu, "Guiding and emission of milijoule single-cycle THz pulse from laser-driven wire-like targets," Opt. Express **28**, 15258 (2020).
[23]Z. Nie, C.-H. Pai, J. Hua, C. Zhang, Y. Wu, Y. Wan, F. Li, J. Zhang, Z. Cheng, Q. Su, S. Liu, Y. Ma, X. Ning, Y. He, W. Lu, H.-H. Chu, J. Wang, W. B. Mori, and C. Joshi, "Relativistic single-cycle tunable infrared pulses generated from a tailored plasma density structure," Nat. Photonics **12**, 489–494 (2018).
[24]X.-L. Zhu, M. Chen, S.-M. Weng, P. McKenna, Z.-M. Sheng, and J. Zhang, "Single-cycle terawatt twisted-light pulses at midinfrared wavelengths above 10 $\mu$m," Phys. Rev. Appl. **12**, 054024 (2019).
[25]V. V. Kulagin, V. N. Kornienko, V. A. Cherepenin, D. N. Gupta, and H. Suk, "Characteristics of quasi-unipolar electromagnetic pulses formed in the interaction of high-power laser pulses with nanoscale targets," Quantum Electron. **49**, 788–795 (2019).
[26]Z. Nie, C.-H. Pai, J. Zhang, X. Ning, J. Hua, Y. He, Y. Wu, Q. Su, S. Liu, Y. Ma, Z. Cheng, W. Lu, H.-H. Chu, J. Wang, C. Zhang, W. B. Mori, and C. Joshi, "Photon deceleration in plasma wakes generates single-cycle relativistic tunable infrared pulses," Nat. Commun. **11**, 2787 (2020).
[27]A. A. Golovanov and I. Y. Kostyukov, "Generation of IR radiation in the interaction of an ultrashort laser pulse with a gas jet," Quantum Electron. **51**, 850–853 (2021).
[28]V. V. Kulagin, V. N. Kornienko, V. A. Cherepenin, D. N. Gupta, and H. Suk, "Generation of intense coherent electromagnetic radiation during the interaction of a multi-terawatt laser pulse with a nanowire target," Quantum Electron. **51**, 323–332 (2021).
[29]E. Siminos, I. Thiele, and C. Olofsson, "Laser wakefield driven generation of isolated carrier-envelope-phase tunable intense subcycle pulses," Phys. Rev. Lett. **126**, 044801 (2021).
[30]X.-L. Zhu, W.-Y. Liu, S.-M. Weng, M. Chen, Z.-M. Sheng, and J. Zhang, "Generation of single-cycle relativistic infrared pulses at wavelengths above 20 $\mu$m from density-tailored plasmas," Matter Radiat. Extremes **7**, 014403 (2022).
[31]A. V. Mitrofanov, D. A. Sidorov-Biryukov, A. A. Voronin, A. Pugžlys, G. Andriukaitis, E. A. Stepanov, S. Ališauskas, T. Flöri, A. B. Fedotov, V. Y. Panchenko, A. Baltuška, and A. M. Zheltikov, "Subterawatt femtosecond pulses in the mid-infrared range: New spatiotemporal dynamics of high-power electromagnetic fields," Phys.-Usp. **58**, 89–94 (2015).
[32]D. J. Wilson, A. M. Summers, S. Zigo, B. Davis, S.-J. Robatjazi, J. A. Powell, D. Rolles, A. Rudenko, and C. A. Trallero-Herrero, "An intense, few-cycle source in the long-wave infrared," Sci. Rep. **9**, 6002 (2019).
[33]A. V. Mitrofanov, D. A. Sidorov-Biryukov, P. B. Glek, M. V. Rozhko, E. A. Stepanov, A. D. Shutov, S. V. Ryabchuk, A. A. Voronin, A. B. Fedotov, and A. M. Zheltikov, "Chirp-controlled high-harmonic and attosecond-pulse generation via coherent-wake plasma emission driven by mid-infrared laser pulses," Opt. Lett. **45**, 750 (2020).
[34]A. V. Mitrofanov, D. A. Sidorov-Biryukov, M. V. Rozhko, A. A. Voronin, P. B. Glek, S. V. Ryabchuk, E. E. Serebryannikov, A. B. Fedotov, and A. M. Zheltikov, "Relativistic nonlinear optical phenomena in the field of subterawatt laser pulses," JETP Lett. **112**, 17–23 (2020).
[35]A. V. Mitrofanov, D. A. Sidorov-Biryukov, A. A. Voronin, M. V. Rozhko, P. B. Glek, M. M. Nazarov, E. E. Serebryannikov, A. B. Fedotov, and A. M. Zheltikov, "Enhancement of plasma nonlinearities and generation of a microwave–terahertz supercontinuum in the field of subterawatt mid-infrared pulses," JETP Lett. **113**, 301–307 (2021).
[36]V. V. Meshcherinov, M. V. Spiridonov, V. A. Kazakov, and A. V. Rodin, "Lidar-based remote infrared gas sensor for monitoring anthropogenic pollution: A proof of concept," Quantum Electron. **50**, 1055–1062 (2020).
[37]M. G. Pullen, B. Wolter, A.-T. Le, M. Baudisch, M. Hemmer, A. Senftleben, C. D. Schröter, J. Ullrich, R. Moshammer, C. D. Lin, and J. Biegert, "Imaging an aligned polyatomic molecule with laser-induced electron diffraction," Nat. Commun. **6**, 7262 (2015).
[38]M. Schultze, E. M. Bothschafter, A. Sommer, S. Holzner, W. Schweinberger, M. Fiess, M. Hofstetter, R. Kienberger, V. Apalkov, V. S. Yakovlev, M. I. Stockman, and F. Krausz, "Controlling dielectrics with the electric field of light," Nature **493**, 75–78 (2013).
[39]H.-T. Chang, A. Guggenmos, S. K. Cushing, Y. Cui, N. U. Din, S. R. Acharya, I. J. Porter, U. Kleineberg, V. Turkowski, T. S. Rahman, D. M. Neumark, and S. R. Leone, "Electron thermalization and relaxation in laser-heated nickel by few-femtosecond core-level transient absorption spectroscopy," Phys. Rev. B **103**, 064305 (2021).
[40]S. V. Bulanov, N. M. Naumova, and F. Pegoraro, "Interaction of an ultrashort, relativistically strong laser pulse with an overdense plasma," Phys. Plasmas **1**, 745–757 (1994).
[41]N. M. Naumova, J. A. Nees, I. V. Sokolov, B. Hou, and G. A. Mourou, "Relativistic generation of isolated attosecond pulses in a $\lambda^3$ focal volume," Phys. Rev. Lett. **92**, 063902 (2004).
[42]J. H. Bin, M. Yeung, Z. Gong, H. Y. Wang, C. Kreuzer, M. L. Zhou, M. J. V. Streeter, P. S. Foster, S. Cousens, B. Dromey, J. Meyer-Ter-Vehn, M. Zepf, and J. Schreiber, "Enhanced laser-driven ion acceleration by superponderomotive electrons generated from near-critical-density plasma," Phys. Rev. Lett. **120**, 074801 (2018).

[43]P. Hilz, T. M. Ostermayr, A. Huebl, V. Bagnoud, B. Borm, M. Bussmann, M. Gallei, J. Gebhard, D. Haffa, J. Hartmann, T. Kluge, F. H. Lindner, P. Neumayr, C. G. Schaefer, U. Schramm, P. G. Thirolf, T. F. Rösch, F. Wagner, B. Zielbauer, and J. Schreiber, "Isolated proton bunch acceleration by a petawatt laser pulse," Nat. Commun. **9**, 423 (2018).

[44]W. J. Ma, I. J. Kim, J. Q. Yu, I. W. Choi, P. K. Singh, H. W. Lee, J. H. Sung, S. K. Lee, C. Lin, Q. Liao, J. G. Zhu, H. Y. Lu, B. Liu, H. Y. Wang, R. F. Xu, X. T. He, J. E. Chen, M. Zepf, J. Schreiber, X. Q. Yan, and C. H. Nam, "Laser acceleration of highly energetic carbon ions using a double-layer target composed of slightly underdense plasma and ultrathin foil," Phys. Rev. Lett. **122**, 014803 (2019).

[45]N. Zhao, J. Jiao, D. Xie, H. Zhou, S. Zhang, Y. Lang, D. Zou, and H. Zhuo, "Near-100 MeV proton acceleration from $10^{21}$ W/cm$^2$ laser interacting with near-critical density plasma," High Energy Density Phys. **37**, 100889 (2020).

[46]S. Shokita, A. Yogo, S. R. Mirfayzi, Y. Honoki, D. Golovin, T. Ishimoto, Z. Lan, K. Matsuo, T. Mori, K. Okamoto, H. Nagatomo, H. Nishimura, Y. Sentoku, K. Yamanoi, and R. Kodama, "Observation of MeV-energy ions from the interaction of over picosecond laser pulses with near-critical density foam targets," High Energy Density Phys. **36**, 100821 (2020).

[47]I. Göthel, C. Bernert, M. Bussmann, M. Garten, T. Miethlinger, M. Rehwald, K. Zeil, T. Ziegler, T. E. Cowan, U. Schramm, and T. Kluge, "Optimized laser ion acceleration at the relativistic critical density surface," Plasma Phys. Controlled Fusion **64**, 044010 (2022).

[48]A. A. Gonoskov, A. V. Korzhimanov, A. V. Kim, M. Marklund, and A. M. Sergeev, "Ultrarelativistic nanoplasmonics as a route towards extreme-intensity attosecond pulses," Phys. Rev. E **84**, 046403 (2011).

[49]A. Gonoskov, "Theory of relativistic radiation reflection from plasmas," Phys. Plasmas **25**, 013108 (2018).

[50]I. A. Surmin, S. I. Bastrakov, E. S. Efimenko, A. A. Gonoskov, A. V. Korzhimanov, and I. B. Meyerov, "Particle-in-Cell laser-plasma simulation on Xeon Phi coprocessors," Comput. Phys. Commun. **202**, 204–210 (2016).

[51]V. I. Eremin, A. V. Korzhimanov, and A. V. Kim, "Relativistic self-induced transparency effect during ultraintense laser interaction with overdense plasmas: Why it occurs and its use for ultrashort electron bunch generation," Phys. Plasmas **17**, 043102 (2010).

[52]E. Siminos, M. Grech, S. Skupin, T. Schlegel, and V. T. Tikhonchuk, "Effect of electron heating on self-induced transparency in relativistic-intensity laser-plasma interactions," Phys. Rev. E **86**, 056404 (2012).

[53]E. Siminos, M. Grech, B. S. Wettervik, and T. Fülöp, "Kinetic and finite ion mass effects on the transition to relativistic self-induced transparency in laser-driven ion acceleration," New J. Phys. **19**, 123042 (2017).

[54]N. A. Mikheitsev and A. V. Korzhimanov, "Effect of finite ion mass on relativistic self-induced transparency of plasma layers with a sharp boundary," Quantum Electron. **50**, 776–781 (2020).

[55]S. V. Bulanov, N. M. Naumova, T. Z. Esirkepov, and F. Pegoraro, "Evolution of the frequency spectrum of a relativistically strong laser pulse in a plasma," Phys. Scr. **1996**, 258.

[56]A. Sakharov, N. Naumova, and S. Bulanov, "Spectra of backward stimulated Raman scattering of short relativistically strong laser pulses in an underdense plasma," Plasma Phys. Rep. **24**, 818–824 (1998).

[57]J. G. Moreau, E. d'Humières, R. Nuter, and V. T. Tikhonchuk, "Stimulated Raman scattering in the relativistic regime in near-critical plasmas," Phys. Rev. E **95**, 013208 (2017).